LIMNOLOGY
and
OCEANOGRAPHY

ASLO

Limnol. Oceanogr. 62, 2017, 75–88

doi: 10.1002/lno.10373

Co-existence of distinct *Ostreococcus* ecotypes at an oceanic front

Sophie Clayton,[1,a]* Yun-Chi Lin,[2,3,4] Michael J. Follows,[1] Alexandra Z. Worden[2,3,5]
[1]Massachusetts Institute of Technology, Cambridge, Massachusetts
[2]Monterey Bay Aquarium Research Institute, Moss Landing, California
[3]Department of Ocean Sciences, University of California Santa Cruz, Santa Cruz, California
[4]Institute of Marine Biology, National Taiwan Ocean University, Keelung, Taiwan, R.O.C.
[5]Integrated Microbial Biodiversity Program, Canadian Institute for Advanced Research, Toronto, Ontario, Canada

Abstract

Western boundary currents support high primary production and carbon export. Here, we performed a survey of photosynthetic picoeukaryotes in the North Pacific Ocean in four transects crossing the Kuroshio Front. Prasinophyte algae comprised 85% of 18S rRNA gene sequences for photosynthetic taxa in the <5 μm size fraction. The picoplanktonic (<2 μm) genera *Micromonas* and *Ostreococcus* comprised 30% and 51% of the total photosynthetic 18S rDNA sequences from five stations. Phylogenetic analysis showed that two *Ostreococcus* ecotypes, until now rarely found to co-occur, were both present in the majority of samples. *Ostreococcus* ecotype OI reached $6{,}830 \pm 343$ gene copies mL^{-1}, while *Ostreococcus* ecotype OII reached $50{,}190 \pm 971$ gene copies mL^{-1} based on qPCR analysis of the 18S rRNA gene. These values are higher than in studies of other oceanographic regions by a factor of 10 for OII. The data suggest that meso- and finer-scale physical dynamics had a significant impact on the populations at the front, either by mingling ecotypes from different source regions at fine scales (~10s km) or by stimulating their growth through vertical nutrient injections. We investigate this hypothesis with an idealized diffusion-reaction model, and find that only a combination of mixing and positive net growth can explain the observed distributions and overlap of the two *Ostreococcus* ecotypes. Our field observations support larger-scale numerical ocean simulations that predict enhanced biodiversity at western boundary current fronts, and suggest a strategy for systematically testing that hypothesis.

Open ocean fronts are characterized by steep density gradients and have profound influences on marine systems. They can act as boundaries between distinct biomes, e.g., distinct biogeographical regions supporting different biological communities, such as the subpolar and subtropical gyres (Bower et al. 1985). Fronts can also be sites of enhanced vertical turbulence supplying nutrients to the euphotic zone (Pollard and Regier 1992; Nagai et al. 2009; Kaneko et al. 2013). High rates of primary production (Palevsky et al. 2013), elevated phytoplankton biomass (Baird et al. 2008; Chekalyuk et al. 2012) and enhanced export of organic matter (Allen et al. 2005; Omand et al. 2015) are also associated with frontal zones. Recent observations from the North Pacific (Ribalet et al. 2010; Taylor et al. 2012) as well as a remote sensing study of the Brazil-Malvinas confluence zone (D'Ovidio et al. 2010) and numerical simulations of global phytoplankton populations (Barton et al. 2010; Clayton et al. 2013) suggest that western boundary current fronts create sites of elevated phytoplankton biodiversity. The hypothesized mechanism invokes convergence of seed populations from distinct, upstream biomes, and fertilization (Clayton et al. 2013) associated with the outcropping of subsurface nutrient streams along with enhanced vertical mixing. *In situ* data of appropriate physical and biological resolution to address this hypothesis are rare. In particular, although several studies have advanced knowledge considerably in terms of bulk biogeochemical properties (e.g., biomass, productivity and export), species-level resolution of phytoplankton distributions has not been available. Species-level differentiation provides insight into the niche and habitat constraints of the taxa

*Correspondence: sclayton@uw.edu

[a]Present address: School of Oceanography, University of Washington, Seattle, Washington.

Additional Supporting Information may be found in the online version of this article.

present and is therefore an important component of understanding fertilization effects that occur in such regions.

The Kuroshio Extension front, located along the eastward flowing arm of the Kuroshio western boundary current in the North Pacific, separates subtropical and subpolar waters. It is a region of high productivity and an important foraging ground for higher trophic levels (Mugo et al. 2014). A handful of high-resolution studies of the phytoplankton assemblages at the Kuroshio Extension front have largely focused on microphytoplankton (>10 μm) using microscope-based taxonomy (Yamamoto 1986; Yamamoto et al. 1988). Yamamoto et al. (1988) characterized the microphytoplankton communities in three sections across the front, to the south and east of Japan, and performed a cluster analysis which revealed three distinct assemblages: two from the biomes associated with the subtropical and subpolar gyres bordering the front, as well as a cluster unique to the front itself, the members of which suggested the entrainment of neritic species into the stream. A more recent survey, about 500 km further downstream, included microscopic taxonomy of microphytoplankton (>10 μm), flow cytometric enumeration of picophytoplankton (with diameters likely ranging from 0.5 – 10 μm) and HPLC pigments extracted from whole seawater (Clayton et al. 2014a). In that study, a similar cluster analysis revealed just two distinct assemblages representing the surrounding biomes without the third, frontal assemblage observed by Yamamoto et al. (1988). These studies show that the front acts to structure phytoplankton communities, but it is still unclear how the physical dynamics of the front are linked to the observed phytoplankton species distributions.

Molecular methods allow plankton populations to be described and examined at an even finer taxonomic resolution, beyond functional group and species. This is particularly relevant for the pico- (<2 μm) and nano-phytoplankton (<10 μm) which account for a large portion of the total phytoplankton biomass and primary productivity in this region (Nishibe et al. 2014). Eukaryotic pico- and nanophytoplankton are highly diverse (Vaulot et al. 2008; Massana 2011; Worden et al. 2015), yet species or ecotype assemblages cannot be distinguished by morphology or pigments. Molecular characterization of picoplankton communities can provide a powerful tool for revealing and interpreting the role of physical dispersal in shaping assemblages and biodiversity at ocean fronts, so long as the region is sampled at a physical (spatial) resolution fine enough to capture frontal dynamics. Molecular methods have been used to characterize large-scale biogeographical patterns in distributions of picocyanobacteria (Johnson et al. 2006; Kashtan et al. 2014) and picoeukaryotes, e.g., (Cuvelier et al. 2010; Shi et al. 2011; Kirkham et al. 2013). These reveal sorting of related ecotypes over environmental gradients at the gyre- and basin-scale (1000s km). Additionally, a study of bacterioplankton populations that followed ocean drifters found that bacterial assemblages are also likely shaped by, or associated with, mesoscale physical circulations (e.g., oceanic mesoscale eddies) on the order of 10s of kilometers (Hewson et al. 2006). In connection to physical data this kind of information provides a tool with which to address hypotheses on mechanisms driving biodiversity at fronts.

In this study, we characterize eukaryotic phytoplankton populations at the molecular level in the context of hydrographic data from a high-resolution (< 10 km between stations) survey across the Kuroshio Extension front. Our study utilizes samples from an expedition where physical (Nagai et al. 2012) and biogeochemical properties have been previously described, and flow cytometry-based cell counts demonstrated that small photosynthetic picoeukaryotes were abundant (up to ~15,000 cells mL^{-1}) in the vicinity of the front (Clayton et al. 2014a). We used the results of targeted quantitative PCR (qPCR) enumeration of distinct *Ostreococcus* ecotypes to explore the hypothesis that open ocean fronts support high levels of biodiversity by mingling and fertilizing distinct communities. These genetically distinct *Ostreococcus* have been termed coastal (or mesotrophic) and oceanic ecotypes, based on their distributions in the field (Demir-Hilton et al. 2011; Simmons et al. 2016). Together, the high-resolution physical and biological data from the Kuroshio Extension, alongside inferences from an idealized reaction-diffusion model integrating these data, reveal the interplay of physical mixing and biological processes in shaping the picoeukaryotic community at that front. Our studies indicate that the physical dynamics of the front mediate co-existence and support elevated biodiversity.

Methods

Study site and sample collection

A physical, biological and chemical survey of the Kuroshio Extension region of the North Western Pacific Ocean was undertaken aboard the R/V Natsushima (JAMSTEC) in October 2009. The front was crossed five times (Fig. 1). A CTD (Advantech Ltd.) equipped with Niskin bottles was deployed at eight stations along each transect, roughly 9 km apart. Stations were numbered from 1 to 41 and are referred to by the transect and station number, e.g., A8 (Fig. 1). Discrete seawater samples were collected from 5 depths at each station for dissolved nutrients. Sampling along each transect was completed within 18 hours from start to finish with approximately 6 hours between transects in order to minimize aliasing due to environmental variability.

Eukaryotic community composition analysis

DNA was collected from the sea surface at a total of 26 stations along transects A, B, D and E (Fig. 1). We pre-filtered 1 L of whole seawater through a 5 μm 47 mm filter and then onto a 0.8 μm 25 mm filter (both Millipore Durapore). Additionally, at Station A1, DNA samples were collected at depths of 25, 48, 75 and 150 m. The filters were placed in 1.2 mL

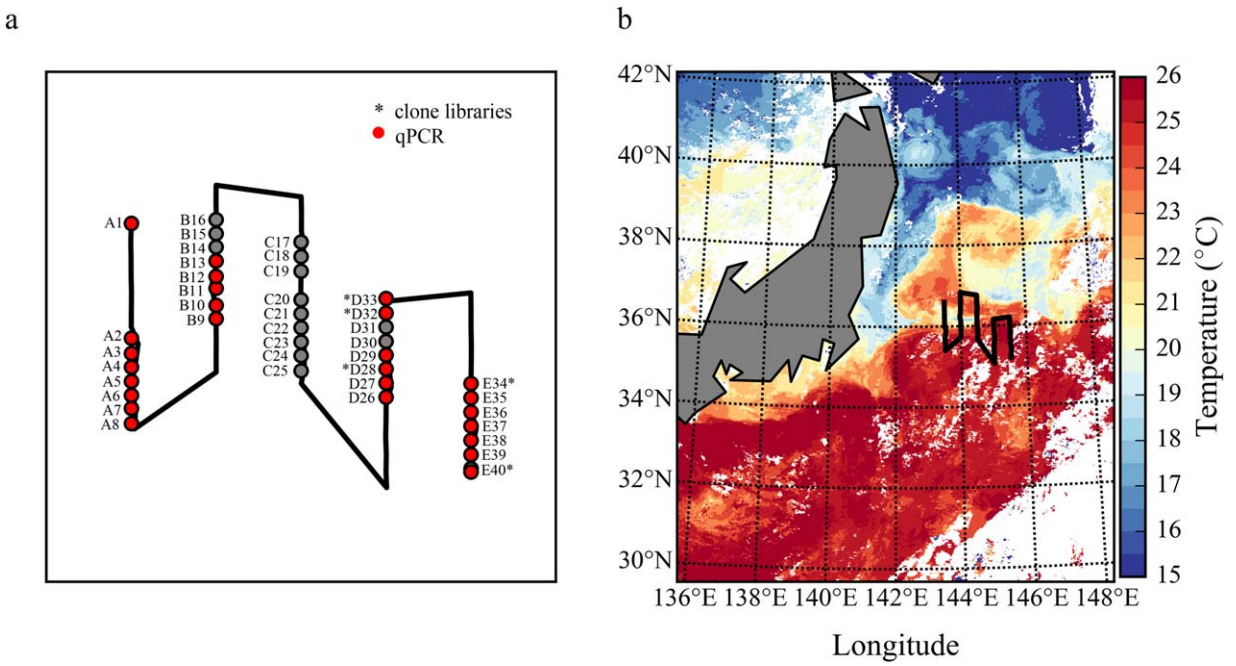

Fig. 1. The cruise track and sample stations are shown in panel (**a**), with the sample stations used for clone libraries (asterisk) and qPCR (red) highlighted. NOAA Sea surface temperature (SST) for the study region and surrounding area on 20 October 2009 (**b**), with the cruise track indicated in black for context. The Oyashio current can be seen as the band of cold waters (< 17°C) found just off the east coast of Japan, and the Kuroshio current as a strong temperature front to the south and east of Japan. Although useful for setting the large scale context of the study region, a daily snapshot of SST is somewhat misleading for looking at the individual properties at each station. The Kuroshio Extension region is highly dynamic, and our stations are very closely spaced, so the temperature and salinity at any given point in space varied greatly over the duration of the cruise (one week). The *in situ* temperature and salinity for each station can be found in Table 1.

Nalgene cryovials with 500 μL of Qiagen RNAlater and immediately frozen (and stored) at −80°C until extraction.

Environmental clone library construction and sequencing

DNA extraction was conducted using a modification of the DNeasy Plant Kit (Qiagen) with additional freeze-thaw and bead beating steps to ensure effective cell lysis (Cuvelier et al. 2010; Demir-Hilton et al. 2011). Clone libraries were constructed for surface water samples from stations D28, D32, D33, E34 and E40, using PCR primers targeting the 18S rRNA gene (EUKf: 5′-ACCTGGTTGATCCTGCCAG-3′; EUKr: 5′-TGATCCTTYGCAGGTTCAC-3′) that complement conserved regions of the 5′ and 3′ termini of the gene (Moon-Van Der Staay et al. 2001). PCR conditions were as in Worden (2006) and the products were directly cloned using the TOPO TA cloning kit (Invitrogen). Ninety six clones were randomly picked for sequencing, rendering 65 to 84 successful sequences for each of the 5 libraries constructed. Sequencing was performed on a 3730xl DNA Analyzer (Applied Biosystems) using the internal primer, EUK502f (5′-GGAGGGCAAGTCTGGT-3′) to obtain partial sequences with an average length of 833 nt.

Sequence analysis and phylogenetics

Initial assignment of environmental sequences to known taxa and uncultured environmental groups was performed using BLASTn to NCBI nr with default settings. Sequences from taxa with high representation were clustered at the >99% identity level. Representative sequences were used for phylogenetic analysis of prasinophytes and additional 18S rRNA gene sequences were acquired from GenBank, with attention to a recent analysis of cultured prasinophytes (Marin and Melkonian 2010). Almost all sequences analyzed in the former study were included, but other key Mamiellophyceae sequences from environmental samples (and some cultures) were added. Alignments were performed using ClustalW (Larkin et al. 2007) and manually adjusted as necessary. Ambiguously aligned positions were removed prior to phylogenetic analysis resulting in 781 nucleotide positions in the final (masked) alignment. Two maximum-likelihood methods were employed, a true ML analysis (100 bootstrap replicates) and an approximate likelihood (SH-like support, 1000 replicates), both in PhyML v3 (Guindon et al. 2010). Neighbor-joining distance analysis was also performed in Phylip (Felsenstein 2005) with 100 bootstrap replicates.

qPCR quantification of *Ostreococcus* ecotypes

Two Taqman primer-probe sets were employed to enumerate the 18S rDNA copy numbers of the *Ostreococcus* OI and OII ecotypes (Demir-Hilton et al. 2011). The former amplifies Clades A and C *Ostreococcus*, *sensu* Guillou et al.

(2004), and the latter Clade B. Total qPCR reaction volumes were 25 μL, including 12.5 μL Taqman universal PCR Master Mix, 2.5 μL of probes (250 nM final concentration), 2.5 μL of forward and reverse primers (900 nM final concentration), 3 μL H_2O and 2 μL environmental DNA. Technical triplicates were performed and an additional reaction for each sample was used for testing PCR inhibition levels. Inhibition tests were performed by spiking the additional reaction for each environmental template with 2 μL plasmid (10^4 or 10^5 copies well^{-1}). If the C_T (threshold cycles) values on spiking were higher than those from the standard curve, we assume inhibition in environmental samples. The formula for calculating PCR inhibition is given below:

$$\left[1-\left(\frac{C_T \text{ sample}-C_T \text{ } 10^{4\text{ or }5}\text{plasmid}}{C_T \text{ } 10^{4\text{ or }5}\text{plasmid}}\right)\right]\times 100\% \qquad (1)$$

For values ranging from 96 to 110%, we conclude that no inhibition existed. However, for values higher than 110%, inhibition may have been caused by low plasmid concentration on spiking. In this case, we repeat the measurements with a higher plasmid addition (10^5 copies well^{-1}). If a 10x diluted environmental sample showed inhibition (<96%), then it was subsequently diluted to 100x. Standard curves were created using triplicate reactions for copy number standards (from 1 to 10^8 copies well^{-1} and 10-fold dilution series). An AB7500 was used with an initial step of 95°C for 10 min and 45 cycles of 95°C (15 sec) and 60°C (1 min). qPCR plate runs were considered successful if the R^2 of the standard curve was >99% and no inhibition was observed. Gene-copy enumeration was robust to ≥10 copies well^{-1}. Detection limits calculated from filtration volume, elution volume, final DNA dilution and qPCR detection levels from the standard curve were 0.25–2.63 copies mL^{-1}.

Data deposition

The sequences reported in this paper have been deposited in GenBank (accession nos. KT012724 to KT013052). Environmental, nutrient, phytoplankton abundance and photosynthetic pigment data have all been submitted to the Pangaea database (Clayton et al. 2014b).

Results

Eukaryotic phytoplankton communities at the sea surface were surveyed at five stations: D28, D32, D33, E34 and E40. The *in situ* temperature and salinity data for these stations is given in Table 1. For reference, the characteristic salinity ranges of Oyashio and Kuroshio water masses are <33.5 psu and >34.2 psu, respectively (Yamamoto et al. 1988). Thus, these stations represent a range of conditions along the mixing gradient between the Oyashio and Kuroshio end-member water masses brought together at the front, from fresher and cooler (D32, D33), to intermediate (D28, E34), and warmer and saltier (E40). Because photosynthetic picoeukaryotes were abundant during the study period (Clayton et al. 2014a), 18S rRNA gene clone libraries were constructed from the <5 μm size fraction. The photosynthetic taxa and non-pigmented taxa identified in the 18S rRNA gene data accounted for 41% and 59% of the total clones, respectively (Table 2). Prasinophytes accounted for 33% on average of the total sequences in our study (133/387) and prasinophyte algae belonging to the Mamiellophyceae class comprised the majority of sequences recovered from photosynthetic taxa (Fig. 2, Table 2). Specifically, the picoeukaryotic genera *Ostreococcus* and *Micromonas* comprised 51% and 30%, respectively, of the 18S rRNA gene sequences from known photosynthetic taxa. Syndiniales, metazoa (presumably from broken body parts) and Marine Stramenopiles (MASTs) constituted the major components in non-pigmented sequences. Syndiniale sequences appeared to be more abundant in warm waters at stations of E34 and E40 (Table 2).

Phylogenetic analysis revealed that multiple clades of *Micromonas* and *Ostreococcus* were present. Moreover, several clades from each genus were often co-located (Fig. 2). For example, *Micromonas* Clade AB.I was recovered at all stations and *Micromonas* Clade E.1 was often co-located with Clade AB.I. These clades encapsulate species level differences based on comparative genomics (van Baren et al. 2016, Worden et al. 2009) and marker gene analyses (Slapeta et al. 2006; Worden 2006; Simmons et al. 2015). No sequences were recovered related to *Ostreococcus tauri*, which was isolated from an oyster lagoon (Courties et al. 1994), or *Ostreococcus* Clade D (e.g., RCC501), which has now been described as a separate species, *Ostreococcus mediterraneus* (Subirana et al. 2013). However, at four of the five stations investigated both *Ostreococcus* OI and OII were found.

Distribution of *Ostreococcus* ecotypes and relationship to environmental parameters

Because *Ostreococcus* OI and OII have previously only been reported to co-occur in the North West Atlantic Shelf Break Front (Demir-Hilton et al. 2011), we quantified OI and OII abundances based on 18S rRNA gene copies mL^{-1} along four cross-front transects (A, B, D and E) that encapsulated distinct dynamical features found along and across the front.

The qPCR measurements allowed us to move beyond qualitative information reflected by 18S rRNA gene sequencing, to high sensitivity numerical data. Strikingly, both *Ostreococcus* ecotypes were detected in 54% of the surface samples, and 46% of the surface samples contained >10 copies mL^{-1} of both *Ostreococcus* ecotypes. OII was detected in all 26 surface samples investigated, while OI was detected in 14 stations, and quantifiable in 12 stations (Table 1, Fig. 3). Contributions of the two ecotypes were not necessarily balanced at the 12 stations where co-occurrence was observed, but in each case were present well above detection levels (OI: 2 and OII: 1 gene copies mL^{-1}; Table 1). Taken together, qPCR-based *Ostreococcus* cell numbers accounted for 25–68% of the

Table 1. Abundances of *Ostreococcus* ecotypes, temperature and salinity at each station. Where the depth is not specified, the sample was taken at the sea surface. Asterisks denote samples where *Ostreococcus* ecotype OI was detected but not quantifiable.

			(18S gene copies mL^{-1})			
Station (depth)	Longitude (° W)	Latitude (° N)	OI ± std	OII ± std	Temperature (°C)	Salinity (psu)
A1 (0m)	143.48	36.61	1 ± 1*	11012 ± 3409	23.76	34.19
A1 (25m)	143.48	36.61	0 ± 0	8352 ± 775	23.72	34.22
A1 (48m)	143.48	36.61	0 ± 0*	546 ± 25	21.81	34.22
A1 (75m)	143.48	36.61	3 ± 4*	85 ± 28	18.86	34.47
A1 (150m)	143.48	36.61	0 ± 0	240 ± 69	13.84	34.52
A2	143.53	35.93	5007 ± 975	32942 ± 809	22.97	34.09
A3	143.53	35.84	12 ± 5	31110 ± 1181	24.13	33.72
A4	143.53	35.76	0 ± 0	6462 ± 283	24.87	34.19
A5	143.53	35.68	0 ± 0	11402 ± 517	25.24	34.19
A6	143.53	35.6	0 ± 0	3996 ± 49	25.38	34.14
A7	143.52	35.52	0 ± 0	628 ± 60	25.17	33.72
A8	143.53	35.43	0 ± 0	233 ± 37	25.10	34.23
B9	144	36.05	3406 ± 233	840 ± 76	20.16	33.70
B10	144	36.13	6826 ± 343	192 ± 33	18.38	33.23
B11	143.97	36.23	6350 ± 455	4200 ± 100	20.99	33.78
B12	143.99	36.3	225 ± 31	50190 ± 971	23.62	33.80
B13	144	36.39	1 ± 1*	36051 ± 834	23.80	34.18
D26	145.08	35.59	0 ± 0	10947 ± 377	24.51	34.21
D27	145.01	35.67	167 ± 58	4972 ± 131	23.08	34.20
D28	145.01	35.75	85 ± 48	7279 ± 100	22.18	34.09
D29	145	35.83	1688 ± 88	424 ± 21	18.04	33.28
D32	145	36.08	1514 ± 105	4862 ± 119	21.15	33.96
D33	145	36.17	3638 ± 167	5227 ± 374	21.32	33.80
E34	145.51	35.67	55 ± 36	8082 ± 488	23.95	34.16
E35	145.53	35.58	0 ± 0	5716 ± 231	24.14	34.25
E36	145.52	35.5	0 ± 0	2641 ± 336	24.14	34.29
E37	145.52	35.42	0 ± 0	2396 ± 123	25.05	34.27
E38	145.5	35.33	0 ± 0	1550 ± 78	24.51	33.43
E39	145.5	35.25	0 ± 0	1613 ± 48	24.51	34.26
E40	145.5	35.17	0 ± 0	909 ± 37	24.51	34.28

picoeukaryote cells enumerated by flow cytometry (Clayton et al. 2014a) at stations where both types of data were available, after taking into account the two 18S rRNA gene copies per genome. *Ostreococcus* ecotype OII gene copies mL^{-1} were generally higher than those of OI. Where OI was detected, its abundance ranged from 3 ± 4 to 6,826 ± 343 18S rRNA gene copies mL^{-1}. The OII ecotype ranged from 85 ± 28 to 50,190 ± 971 18S rRNA gene copies mL^{-1} (Table 1).

Overall, OII 18S rRNA gene copies mL^{-1} was positively correlated with *in vivo* chlorophyll fluorescence levels (Pearson correlation coefficient, $r_p = 0.58$, $p < 0.005$). OII 18S rRNA gene copies mL^{-1} increased in association with locally enhanced nutrient supplies and elevated chlorophyll driven by both the frontal circulation and enhanced vertical mixing at the front (Nagai et al. 2012; Clayton et al. 2014a). In contrast, occurrences of ecotype OI were generally associated with the cooler, lower salinity Oyashio waters and its abundance was negatively correlated with both salinity ($r_p = -0.53$; $p < 0.005$) and temperature ($r_p = -0.73$; $p < 0.001$).

Although OII 18S rRNA gene copies per mL^{-1} were generally higher than OI, the relative abundance of each appeared to be strongly influenced by the originating water mass. Thus, the highest abundances of OI (>3000 18S rRNA gene copies mL^{-1}) were found at stations A2, B10, B11 and D33. These "high OI" stations had a mean salinity of 33.73 psu (±0.31 psu) and mean surface temperature of 20.92°C (±1.65°C). The highest OII abundances (>10,000 18S rRNA gene copies mL^{-1}), were found at stations A1, A2, A3, A5, B12, B13 and D26. These "high OII" stations had a mean salinity of 34.05 psu (±0.19 psu) and mean temperature of 24.0°C (±0.67°C). Although there is some overlap between the "high OI" and "high OII" stations (i.e. at station A2), the

Table 2. Photosynthetic and presumed heterotrophic taxa in environmental clone libraries based on BLASTn assignments in NCBI nr. Closest environmental clone is provided if ≥99% identity and closest cultured organism had <99% identity. Note the names provided for environmental clones below are unique identifiers and can be used to retrieve the sequences in GenBank, and are supplied in Supporting Information Table S1.

Major group	Closest Cult. taxon	Closest Env. clone	D28	D32	D33	E34	E40	Total
Photosynthetic taxa								
Dinoflagellates	*Gymnodinium*	SGUH984 (100%)	0	0	0	2	0	2
Cryptophytes	*Teleaulax*	127-014	1	2	1	0	0	4
Haptophytes	*Chrysochromulina, Phaeocystis*	See supplementary data	5	2	4	1	0	12
Heterokonts	*Bolidomonas, Pelagomonas, Florenciella, Triparma*	SGYP463 (100%), SGUH580 (100%)	0	1	0	3	1	5
Prasinophytes	See Fig. 2		41	41	33	13	5	133
Non-pigmented taxa								
Alveolate	Syndiniales	See supplementary data	20	6	7	21	30	84
	Ciliophora	See supplementary data	4	2	5	5	4	20
Fungi	Unknown (*Powellomyces*,90%)	MB04.9 (96%)	0	0	1	0	0	1
Unknown	putatively fungal	MB07.52 (99–100%), ST3900.020 (99%)	1	1	1	0	2	5
Heterokonts	MAST	See supplementary data	3	17	6	6	10	42
Picozoa	*Picomonas*	See supplementary data	3	0	1	0	1	5
Opisthokonts	Metazoa		3	7	12	18	8	48
	Choanoflagellate	SCGC AAA071-L17 (100%)	1	0	0	0	0	1
Rhizaria		See supplementary data	0	2	3	1	4	10
Telonema		BL040126.Telo.1 (100%), ST3900.021(100%)	0	1	1	2	0	4
Potential chimeras			3	7	1	0	0	11

highest abundances of OI were found in cooler, fresher waters, whereas the highest abundances of OII were found in warmer, saltier waters. It is interesting to note that the highest abundances of either ecotype were found in mixed waters, with temperature and salinity properties intermediate between Kuroshio and Oyashio end-members. Additionally, it should be noted that all of these stations were in close proximity to the front itself, where the temperature and salinity gradients were strongest (Supporting Information Figs. S2 and S3).

The majority of our samples were taken at the sea surface, however, we also analyzed a depth profile at station A1, and found that OII abundance declined significantly below 35 m (Supporting Information Fig. S1, Table 1; OI was detectable but not quantifiable in three of five depths sampled at this station). Combined with depth profile results from a prior study, these findings support the idea that OII depth distributions are more strongly influenced by nutrient availability (Demir-Hilton et al. 2011) than by light availability (Rodriguez et al. 2005).

Discussion

In our study, prasinophytes accounted for 33% on average of the total sequences. This is higher than the average reported (~15%) in a review of published picoeukaryote clone libraries (Massana 2011). Here, most of the prasinophyte sequences were contributed by *Micromonas* and *Ostreococcus*, in fitting with studies of more nutrient rich regions of eastern boundary current systems (Collado-Fabbri et al. 2011; Rii et al. 2016; Simmons et al. 2016) and coastal systems (Guillou et al. 2004; Worden 2006). Our findings add to the accumulating literature that indicates *Micromonas* and *Ostreococcus* are important, characteristic components of picoeukaryotic community at open ocean fronts. While very few other photosynthetic eukaryotes were observed in our clone libraries, Syndiniales clearly dominated sequences from heterotrophic taxa, as seen in many prior size fractionated clone libraries (Guillou et al. 2008; Jephcott et al. 2016). These parasites are widespread in the global oceans, and some are known to parasitize dinoflagellates. The other abundant set of sequences from unicellular taxa belonged to MAST (specifically MAST-1, −3, −4, and −7) several of which are known to be predators of bacteria and presumably other small cells (Massana 2011; Lin et al. 2012; Massana et al. 2014).

Our results revealed fine scale (~10 km) patterns in the abundance and co-occurrence of distinct *Ostreococcus* ecotypes at the Kuroshio Front. These ecotypes represent coastal/mesotrophic (OI) and oceanic (OII) ecotypes, and have rarely been observed at the same site (Worden and Not 2008; Demir-Hilton et al. 2011; Simmons et al. 2016). While it is possible that these *Ostreococcus* ecotypes overlap in other

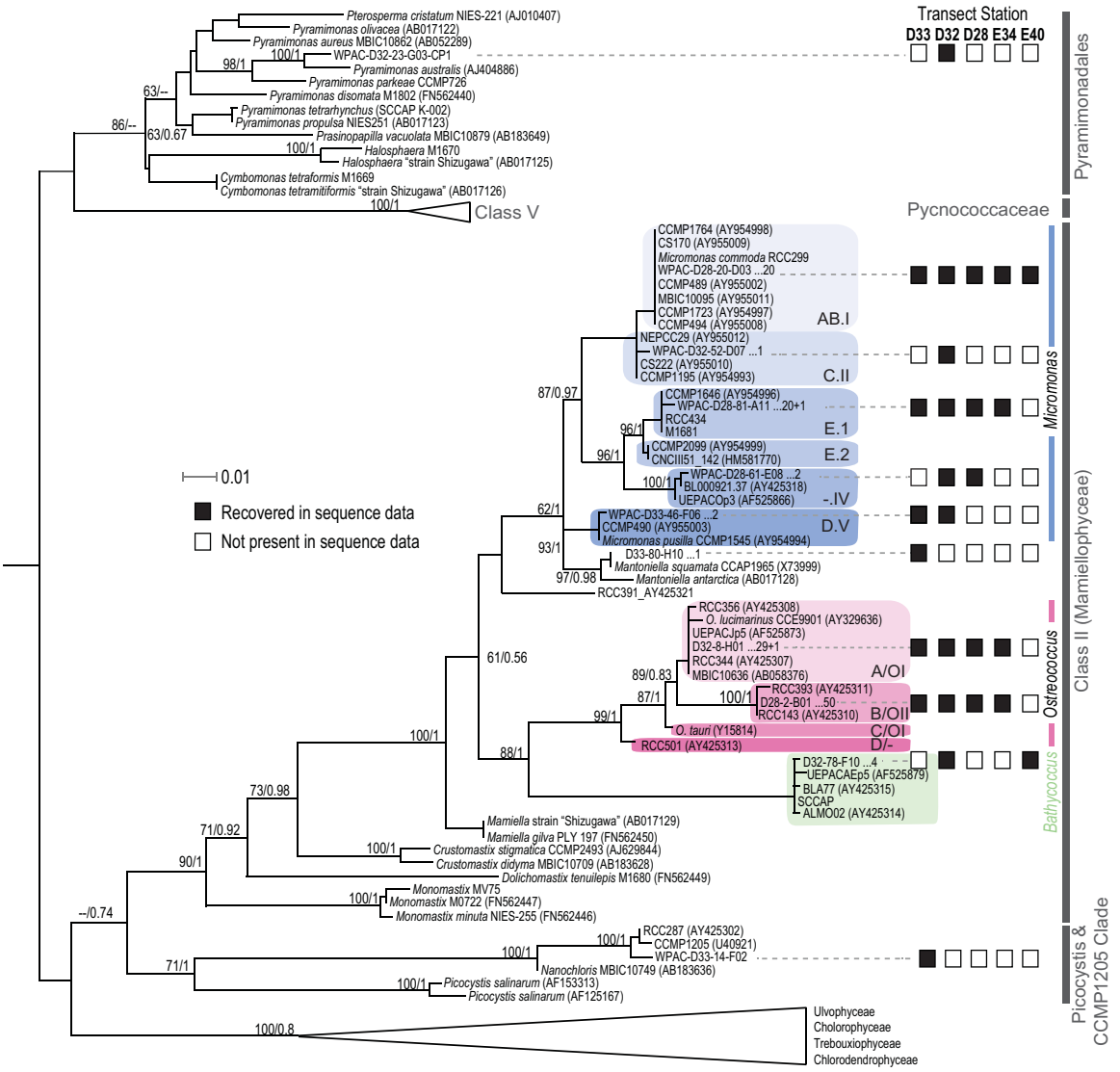

Fig. 2. Prasinophytes in the Kuroshio Extension. Single representatives of each sequence type recovered (clustered at the >99% identity level) in environmental 18S rRNA gene clone libraries from five sites were analysed using maximum likelihood methods. Filled boxes (black) demark stations where the respective sequence was detected and the number of sequences in each cluster is provided beside the clone name (in the tree, see also Table 2). Four *Ostreococcus* clades are highlighted in different shades (pink) and labelled on the interior of shading according to the Clade designations as in (Guillou et al. 2004; Marin and Melkonian 2010) (letters) or the targeting by qPCR primer-probe sets (i.e., OI and OII; Demir-Hilton et al. 2011). Naming of other prasinophyte clades is as defined in (Marin and Melkonian 2010). The reconstruction included all prasinophyte classes, however Classes III and VI, as well as streptophyte green algae at more basal nodes were not recovered in our samples, and therefore are not shown. Node support represents percent support based on Maximum likelihood/Bayesian methods.

regions, to date there is no evidence for such overlap, apart from an observation at the interface of Atlantic coastal waters and the Gulf Stream (Demir-Hilton et al. 2011). Broad scale studies that have used barcoded amplicon sequencing of the V9 18S rRNA gene region do not have the resolution (Monier et al. 2016) to discriminate between the four described *Ostreococcus* clades (Guillou et al. 2004). Relationships of the *Ostreococcus* clades (or OI and OII ecotypes) to depth or location therefore could not be observed in recent V9 18S studies (Monier et al. 2016). Hence, the data presented here provides new insights into environmental distributions of these organisms that cannot be attained from studies of the V9 18S rRNA region. This is important because the ecotypes at hand are distinct based on phylogenies of the 18S rRNA gene (Fig. 2) and Internal Transcribed Spacer (Guillou et al. 2004; Rodriguez et al. 2005; Marin and Melkonian 2010) and have extensive divergence based on complete genome analysis of *O. lucimarinus*, representing Clade A/OI, and RCC809, representing CladeB/OII (Van Baren et al. 2016), in addition to there being few

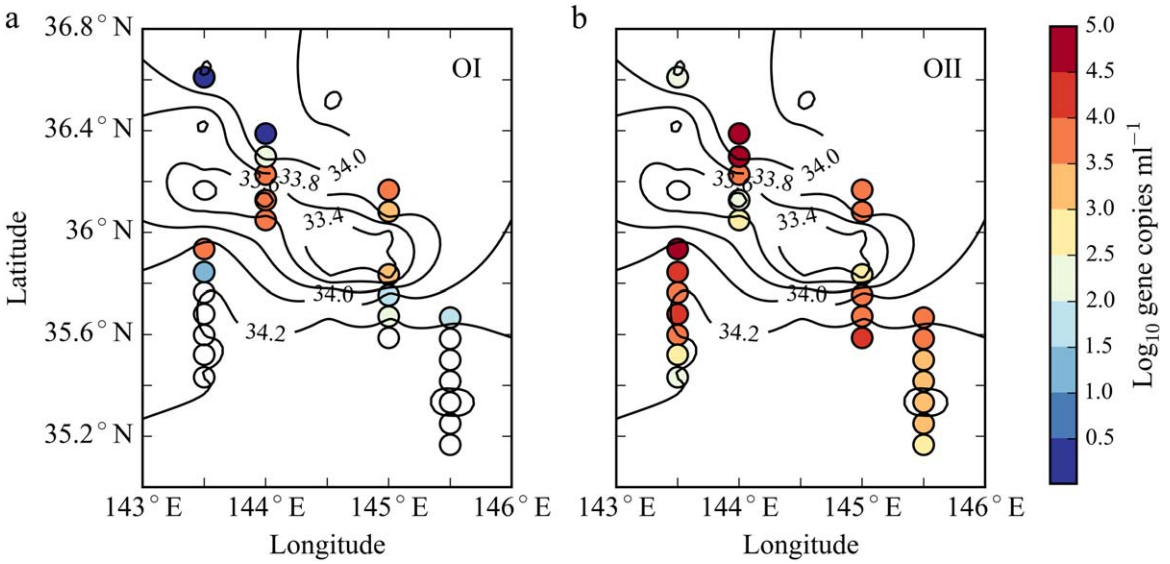

Fig. 3. Abundance of *Ostreococcus* ecotypes OI (**a**) and OII (**b**) as $\log_{10}$ 18S rRNA gene copies mL^{-1}. Stations where that ecotype was not detected by qPCR (empty circles) are also indicated. Salinity contours are represented by black contour lines.

observations of geographic co-location. The combination of highly resolved genetic data, which discriminates between the *Ostreococcus* ecotypes, and high resolution physical sampling in the frontal zone, provides us a window into the role of physical mixing in promoting co-existence.

Here, we observed 20 stations with >1,000 copies mL^{-1} of OII, six stations with >1,000 18S rRNA gene copies mL^{-1} of OI, and four stations with >1,000 18S rRNA gene copies mL^{-1} of both ecotypes. In prior studies, the two ecotypes were quantified in the North Pacific (Simmons et al. 2016) or the North and South Pacific, North and South Atlantic, and abundances of <1,000 18S rRNA gene copies mL^{-1} were observed at the majority of stations, regardless of ecotype. Abundances of the OI ecotype were found to be up to a maximum of ~36,000 18S rRNA gene copies mL^{-1} in the coastal ocean (Simmons et al. 2016), but quickly dropped off to ~1000 18S rRNA gene copies mL^{-1} moving away from the coast in the California Current region. Thus, the OII ecotype abundances observed here exceeded the previously reported maximum abundance of ~5,000 copies mL^{-1} (Demir-Hilton et al. 2011) by a factor of 10. Collectively, these findings allowed us to identify three particularly notable features in our results: (i) both *Ostreococcus* ecotypes co-occurred in a high proportion of samples (54%), (ii) the two ecotypes were present at high abundances, higher than previously reported for OII; (iii) the highest abundances of both ecotypes often occurred at the same stations.

The hydrographic and dynamical context of our study region was very complex, with the influence of physical processes acting at a range of scales. These include the entrainment of fresh Oyashio waters with salinity < 33.5, along the main stream of the Kuroshio Extension, a common feature of this system (Qiu 2001); a filament of warm subtropical water entrained north of the front at the northern end of transect D; and up/downwelling patterns driven by the meandering of the Kuroshio during the study period. Analysis of density fields identified vigorous vertical circulations (> 10 m day^{-1}) along the front, with strong localized upwelling south of the front on transect A and north of the front on transect D, and downwelling at the northern end of transect B and along most of transect E (Nagai et al. 2012).

Examination of the *Ostreococcus* ecotype abundance ratios in temperature-salinity space revealed a clear pattern of mixing between cooler, fresher Oyashio waters dominated by OI and warmer, salter subtropical waters dominated by OII (Fig. 4). The data suggest that as the Oyashio water parcel was transported along the front it was eroded and mixed with Kuroshio water, mingling OI and OII populations. Notably though, similar abundances of both ecotypes were observed at stations B11, D32 and D33 where they were also relatively high (~10,000 18S rRNA gene copies mL^{-1}). These stations were close to the core of the front, where the density gradient was sharpest and the nutricline was domed up towards the surface by upwelling (Supporting Information Figs. S2 and S3).

Perhaps the simplest explanation for the unusual co-occurrence of the ecotypes is the mingling of water masses and the mixing of populations with different upstream origins (Fig. 4). However, the high abundances of both at locations where they co-occurred, relative to published ecotype-specific abundances and "normal" abundances in this region, suggests a more complex situation. At frontal scales (~1–10 km), physical mixing and biological rates (e.g., division rates of phytoplankton cells) are comparable (Lévy

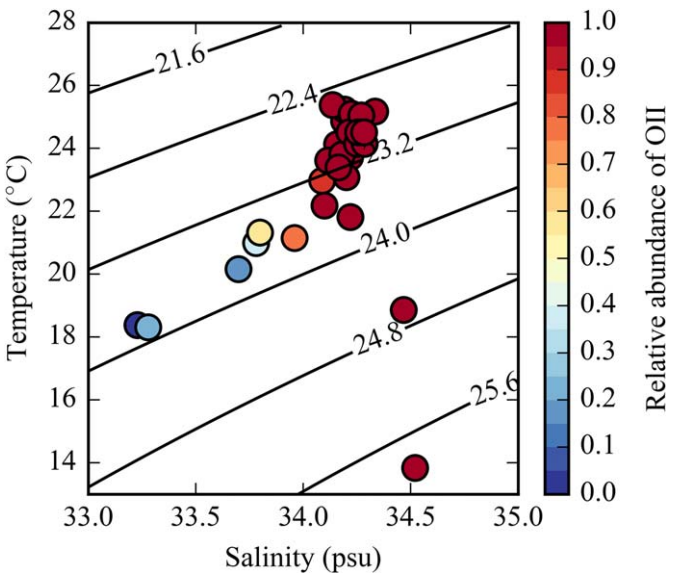

Fig. 4. Temperature/salinity plot of the relative abundance of *Ostreococcus* ecotype OII with respect to the total *Ostreococcus* abundance based on the sum of 18S rRNA gene copies mL^{-1} from the two primer-probe sets used. The sum is considered to reflect the total since the clone libraries only showed the presence of ecotypes that are enumerated by the qPCR primer-probe sets, and the ecological distribution of *O. mediteraneus* thus far appears to be highly restricted (Guillou et al. 2004; Marin and Melkonian 2010). Oyashio waters have a characteristic salinity range <33.5 psu, whereas for Kuroshio it is >34.2 psu.

et al. 2012), and growth and loss processes are just as likely to shape the distribution as physical transport. To provide a synthetic framework in which to consider the interplay of transport and biological processes, we developed a highly idealized model which was designed to elucidate whether the *Ostreococcus* clades: (a) were simply being physically mixed (between their respective origin water masses); (b) if their distributions were driven by biological processes (i.e., active growth and mortality); or (c) a combination of (a) and (b). We described the system as a simple balance of biological "reaction," i.e., net biological growth, and physical "diffusion," representing mixing across the salinity gradient. This is encapsulated as

$$\frac{\partial X_n}{\partial t} = \kappa_S \frac{\partial^2 X_n}{\partial S^2} + \mu_{NET}\ X_n \qquad (2)$$

for $n = 1,2$, and where X_n represents the abundance of *Ostreococcus* (X_1 represents ecotype OI, and X_2 represents ecotype OII), κ_s is the mixing coefficient in salinity space and μ_{NET} is the net biological growth rate, the net effect of growth and mortality (further details are provided in SI Appendix). We cast the model in salinity space (a continuum from fresher to more saline waters) as a way of reducing the complex spatial structure of the front evident in SST data (Fig. 1). Each *Ostreococcus* ecotype is associated with one extreme of the salinity gradient, and each ecotype's distribution is a function of its diffusion along the salinity gradient, and its inherent growth rate.

In this framework, we examined three possible scenarios: (i) Passive mixing of two populations from end member water masses, without significant biological growth or loss ($\mu_{NET} = 0$); (ii) Mixing of two populations that are either fertilized (enhancing growth) or relieved of grazing pressure (reducing mortality losses) leading to positive net growth ($\mu_{NET} > 0$); (iii) Mixing of two populations that, removed from their favored environment, are both declining in population density ($\mu_{NET} < 0$).

For each case, we vary only μ_{NET}, set to be the same for both ecotypes. We based the model end-member concentrations of both ecotypes on their observed abundances, and estimate the value of the mixing coefficient, κ_s, on observed physical data (outlined in the SI appendix). Given the highly dynamic nature of the environment at the front, we examined transient solutions of the model for each experiment. The model was run for 10 days, as this is broadly consistent with the transit time from a coastal region to our study area. The boundary conditions set the background abundance of the two ecotypes at either salinity extreme. S_{min} represents the Oyashio water mass and was set to 33.2, and S_{max} represents the Kuroshio water mass and was set to 34.3. The initial abundances of X_1 and X_2 were set to be zero everywhere but S_{min} and S_{max}, respectively. We based our estimates of μ on measured growth rates of *Ostreoccoccus* strains grown under the same conditions in the lab, which fell within a range of 0.65–0.79 day^{-1} (Schaum et al. 2012). We also took into account field data for picoeukaryote growth (μ) and mortality (m) rates, which yielded net growth rates (μ_{NET}) ranging from 0.20 to 0.81 day^{-1} (Worden et al. 2004). We recognize that loss processes, which are most likely dominated by grazing and viral lysis (Banse 2013), may be better represented by a function which depends on the density of both the predator and the prey. However, little is known about the relative importance of different loss processes on the picoeukarytes, and more work is needed to address this. In the absence of any empirical information regarding the density of predators during our study, the simplest loss model possible (i.e. a timescale which could be associated with any source of mortality) was utilized as we felt it was the most parsimonious and least speculative. Model parameters are listed in Table 3.

Given the complexity of the Kuroshio frontal system, we do not expect our model to exactly reproduce the observations, rather we use it as a conceptual tool to explore which of the proposed scenarios, outlined above, can most plausibly explain our results. The highly idealized model suggests that the second scenario, mixing and population growth ($\mu_{NET} > 0$), is the most consistent with the patterns we observed in the field (Fig. 5a). As suggested by the high population densities of both ecotypes, the model supports the

Table 3. Parameters used in the idealized reaction-diffusion model for each of the three experimental setups.

	Experiment				
Parameter	$\mu_{NET} = 0$	$\mu_{NET}>0$	$\mu_{NET}<0$	**Units**	**Description**
X_1^o	1500	1500	1500	gene copies mL^{-1}	Abundance of X_1 at S_{min}
X_2^o	1500	1500	1500	gene copies mL^{-1}	Abundance of X_2 at S_{max}
μ	0	0.7	0	d^{-1}	Growth rate
m	0	0.1	0.1	d^{-1}	Mortality rate
κ_s	0.5×10^{-7}			s^{-1}	Diffusivity scaled into salinity space

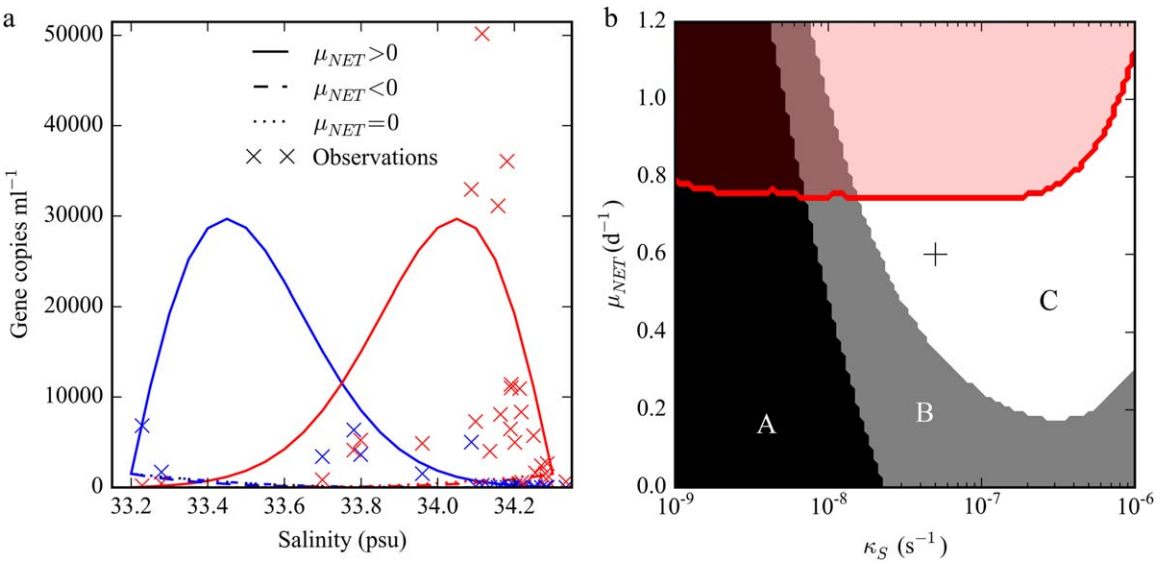

Fig. 5. Results from the reaction-diffusion model (**a**), model results (solid and dashed lines) and observed abundances (crosses) of *Ostreococcus* ecotypes are plotted against salinity. Model results and observations for ecotype OI (blue) and ecotype OII (red) are shown. Sensitivity analysis of the model with respect to κ_S and μ_{NET} (**b**). The three regimes depicted are: (A) no co-existence at S_{mid}, both ecotypes are absent at S_{mid} (X_n (S_{mid}) < 1 gene copies mL^{-1}); (B) co-existence at low abundances, both ecotypes are present at or below their boundary condition abundance at S_{mid} (1 gene copies $mL^{-1} \leq X_n$ (S_{mid}) $\leq X_n{}^0$); (C) co-existence at high abundances, both ecotypes are present above their boundary condition abundance at S_{mid} (X_n (S_{mid}) $> X_n{}^0$). The parameter space which results in very high maximal abundances ($X_n > 10^5$ gene copies mL^{-1}) for both ecotypes is shaded in red, and the parameter combination used to generate the results in the $\mu_{NET} > 0$ experiment panel (a) is denoted by the + symbol.

notion that both ecotypes are (or have very recently been) growing vigorously. This could reflect either stimulation by the turbulent injection of nutrients or a relief of grazing pressure, though it is not possible to determine the underlying cause here. However, a nutrient enrichment would be mechanistically consistent with the hypothesis from ocean models, that western boundary current fronts generate hotspots of phytoplankton diversity through such a combination of physical and biological processes (Clayton et al. 2013).

We also performed an analysis of the sensitivity of the model results to a range of realistic values for κ_S and μ_{NET}. Holding the boundary conditions (X_1^0 and X_2^0) and the model integration time (10 days) constant, we repeated the model integration and classified the result into one of three regimes based on the abundances of both clades at the mid-point of the domain ($S_{mid} = 33.75$). We classify the three regimes in the following way: (A) no co-existence at S_{mid}, both ecotypes are absent at S_{mid} (X_n (S_{mid}) < 1 gene copies mL^{-1}); (B) co-existence at low abundances, both ecotypes are present at or below their boundary condition abundance at S_{mid} (1 gene copies $mL^{-1} \leq X_n$ (S_{mid}) $\leq X_n{}^0$); (C) co-existence at high abundances, both ecotypes are present above their boundary condition abundance at S_{mid} (X_n (S_{mid}) $> X_n{}^0$). We highlight the region of the parameter space that results in very high abundances of both ecotypes, $X_n > 10^5$ gene copies mL^{-1}, roughly twice the maximal abundance of either clade ever observed in the field. This may be an unrealistic result, which could be improved with better parameterization of the biological loss processes. We find that although mixing

appears to be the driving process for generating co-existence of the two ecotypes in the central portion of the domain in this case, higher values of μ_{NET} are necessary to have co-existence *and* high abundances of both ecotypes in the central portion of the domain (Fig. 5b). Thus, the data and model together suggest that the co-occurrence and high abundance of the two *Ostreococcus* ecotypes results from a mingling of populations at the mesoscale, driven by the dynamics of the vigorously unstable front, in combination with local population growth of both ecotypes which may be related to an enhanced nutrient supply in the vicinity of the front also driven by local physics.

We have outlined above the mechanism we expect to be responsible for driving the co-existence of *Ostreococcus* ecotypes observed in our field data. However, the question of how these distinct ecotypes may continue to co-exist once they have been brought into contact remains. Although data exists to show that these ecotypes are genetically distinct and have different biogeographical ranges (Demir-Hilton et al. 2011; Simmons et al. 2016), it is not known what physiological adaptations separate them. It is likely that the co-existence of these ecotypes within the frontal region is a transient feature from a Lagrangian perspective, i.e., following a water parcel along the front, and that one of the two ecotypes will eventually dominate and outcompete the other downstream (Clayton et al. 2013). The exclusion timescale between two phenotypes depends on how close they are in relative fitness, and the bigger the difference in relative fitness, the faster the exclusion timescale (Barton et al. 2010). Co-existence may also be facilitated by the degree of individual variation within each population (Menden-Deuer and Rowlett 2014), which could impact exclusion timescales by affecting the cumulative competitive ability between phenotypes. We do not have sufficient information on the physiologies or genetic diversity of *Ostreococcus* ecotypes to evaluate any measure of their relative fitness. However, since the two ecotypes have only been observed to co-exist in regions where distinct biomes are physically mixed (e.g., the North Atlantic Shelf Break Front, Demir-Hilton et al. (2011); Kuroshio Front, this paper), we suspect that the exclusion timescale is relatively short in oceanographic terms (< years). Since we see co-occurrence driven by mixing, the exclusion timescale must be longer than the mixing timescale, which we estimate to be on the order of ~10 days for the Kuroshio Front (given a characteristic length scale of ~100km, and eddy diffusivity of $\sim 10^4$ m^2 s^{-1}).

Conclusions and outlook

Western boundary currents are the principal conduits for communication between the equatorial and polar regions of the oceans and their resident plankton populations. In the Kuroshio Extension, disparate populations transported by the Kuroshio and Oyashio currents from upstream biomes are brought together, and ultimately mingled as the mesoscale dynamics of the frontal zone stir the different water masses together. The vigorous vertical circulation at the front fertilizes the populations leading to high density populations of organisms from both upstream sources. The mechanism promotes the co-existence of disparate phytoplankton populations at the frontal scale, and is likely to be a feature of other Western Boundary Current frontal zones such as the Gulf Stream and the Brazil-Malvinas Confluence Zone. We hypothesize that this mechanism acts on a wide range of constituents of the phytoplankton community, not just *Ostreococcus* ecotypes. This is consistent with the predictions of global-scale numerical simulations that suggest the study region is likely part of a larger-scale hotspot of diversity (Barton et al. 2010; Clayton et al. 2013). Additionally, the process of mixing and fertilization appears to cause these regions to act as incubators of biodiversity at the basin-scale.

Our highly localized observations provide some mechanistic support for this hypothesis using opportunistic sampling during a survey campaign that was based on physical oceanographic goals. The study provides interesting insight into factors that shape plankton populations at these important oceanographic features and provides a platform for systematic and more comprehensive surveys of western boundary current fronts. Embedding sub-mesoscale (< 10 km) sampling at the front within a coarser grained regional survey which spans the extent of the predicted regional hotspot (100s km) would provide a connection between the local dynamics and wider-scale context. Biodiversity hotspots at western boundary currents are a robust feature of global simulations of marine microbes and yet, to date, only a few microscope-taxonomy based surveys exist to test the prediction. These have led to tantalizing but inconclusive results (Honjo and Okada 1974; Cermeno et al. 2008). Extending the approach taken here, ecotypes of multiple organisms (both eukaryotic and prokaryotic) could be surveyed. Combining genomic and transcriptomic observations would provide measures not only of the abundance of organisms but also their activity (Hunt et al. 2013) and the potential to better define the relative roles of growth and losses. With genetically resolved data and appropriate survey strategies, it will be possible to conclusively determine the presence of these biodiversity hotspots. A better characterization and deeper understanding of these regions will provide insight into the long-term and large-scale biodiversity, stability and function of the planktonic ecosystem. The survey presented here, provides a clear first proof of concept for such a study.

References

Allen, J. T., and others 2005. Diatom carbon export enhanced by silicate upwelling in the northeast Atlantic. Nature. **437**: 728–732. doi:10.1038/nature03948

Baird, M. E., P. G. Timko, J. H. Middleton, T. J. Mullaney, D. R. Cox, and I. M. Suthers. 2008. Biological properties across the Tasman Front off southeast Australia. Deep Sea Res., Part I. **55**: 1438–1455. doi:10.1016/j.dsr.2008.06.011

Banse, K. 2013. Reflections about chance in my career, and on the top-down regulated world. Annu. Rev. Marine Sci. **5**: 1–19. doi:10.1146/annurev-marine-121211-172359

Barton, A. D., S. Dutkiewicz, G. Flierl, J. Bragg, and M. J. Follows. 2010. Patterns of diversity in marine phytoplankton. Science. **327**: 1509–1511 doi:10.1126/science. 1184961

Bower, A. S., H. T. Rossby, and J. L. Lillibridge. 1985. The Gulf Stream - Barrier or Blender? J. Phys. Oceanogr. **15**: 24–32. doi:10.1175/1520-0485(1985)015Ã0024:TGSOBÎ2. 0.CO;2

Cermeno, P., S. Dutkiewicz, R. P. Harris, M. Follows, O. Schofield, and P. G. Falkowski. 2008. The role of nutricline depth in regulating the ocean carbon cycle. Proc. Natl. Acad. Sci. U. S. A. **105**: 20344–20349. doi:10.1073/pnas.0811302106

Chekalyuk, A. M., M. R. Landry, R. Goericke, A. G. Taylor, and M. A. Hafez. 2012. Laser fluorescence analysis of phytoplankton across a frontal zone in the California Current ecosystem. J. Plankton Res. **34**: 761–777. doi:10.1093/plankt/fbs034

Clayton, S., S. Dutkiewicz, O. Jahn, and M. J. Follows. 2013. Dispersal, eddies, and the diversity of marine phytoplankton. l&O:F&E. **3**: 182–197.

Clayton, S., T. Nagai, and M. J. Follows. 2014a. Fine scale phytoplankton community structure across the Kuroshio Front. J. Plankton Res. **36**: 1017–1030. doi:10.1093/plankt/fbu020

Clayton, S., T. Nagai, and M. J. Follows. 2014b. Hydrochemistry, phytoplankton pigment concentration and phytoplankton abundance in water samples obtained in the Kuroshio Extension Front in October 2009. Pangaea. doi:10.1594/PANGAEA.819110

Collado-Fabbri, S., D. Vaulot, and O. Ulloa. 2011. Structure and seasonal dynamics of the eukaryotic picophytoplankton community in a wind-driven coastal upwelling ecosystem. Limnol. Oceanograph. **56**: 2334–2346. doi:10.4319/lo.2011.56.6.2334

Courties, C., A. Vaquer, M. Troussellier, J. Lautier, M. J. Chrétiennot-Dinet, J. Neveux, C. Machado, and H. Claustre. 1994. Smallest eukaryotic organism. Nature. **370**: 255. doi:10.1038/370255a0

Cuvelier, M. L., and others. 2010. Targeted metagenomics and ecology of globally important uncultured eukaryotic phytoplankton. Proc. Natl. Acad. Sci. U. S. A. **107**: 14679–14684. doi:10.1073/pnas.1001665107

Demir-Hilton, E., S. Sudek, M. L. Cuvelier, C. L. Gentemann, J. P. Zehr, and A. Z. Worden. 2011. Global distribution patterns of distinct clades of the photosynthetic picoeukaryote *Ostreococcus*. ISME J. **5**: 1095–1107. doi:10.1038/ismej.2010.209

D'ovidio, F. S., De Monte, S. Alvain, Y. Dandonneau, and M. Levy. 2010. Fluid dynamical niches of phytoplankton types. Proc. Natl. Acad. Sci. U. S. A. **107**: 18366–18370. doi:10.1073/pnas.1004620107

Felsenstein, J. 2005. PHYLIP (Phylogeny Inference Package) version 3.6. Distributed by the author. Department of Genome Sciences, University of Washington, Seattle.

Guillou, L., W. Eikrem, M. J. Chrétiennot-Dinet, F. Le Gall, R. Massana, K. Romari, C. Pedrós-Alió, and D. Vaulot. 2004. Diversity of picoplanktonic prasinophytes assessed by direct nuclear SSU rDNA sequencing of environmental samples and novel isolates retrieved from oceanic and coastal marine ecosystems. Protist. **155**: 193–214. doi:10.1078/143446104774199592

Guillou, L., M. Viprey, A. Chambouvet, R. M. Welsh, A. R. Kirkham, R. Massana, D. J. Scanlan, and A. Z. Worden. 2008. Widespread occurrence and genetic diversity of marine parasitoids belonging to Syndiniales (Alveolata). Environ. Microbiol. **10**: 3349–3365. doi:10.1111/j.1462-2920.2008.01731.x

Guindon, S., J. F. Dufayard, V. Lefort, M. Anisimova, W. Hordijk, and O. Gascuel. 2010. New algorithms and methods to estimate maximum-likelihood phylogenies: assessing the performance of PhyML 3.0. Syst Biol. **59**: 307–321. doi:10.1093/sysbio/syq010

Hewson, I., J. A. Steele, D. G. Capone, and J. A. Fuhrman. 2006. Temporal and spatial scales of variation in bacterioplankton assemblages of oligotrophic surface waters. Mar. Ecol. Prog. Ser. **311**: 67–77. doi:10.3354/meps311067

Honjo, S., and H. Okada. 1974. Community structure of coccolithophores in the photic layer of the mid-Pacific. Micropaleontology. **20**: 209–230. doi:10.2307/1485061

Hunt, D. E., Y. Lin, M. J. Church, D. M. Karl, S. G. Tringe, L. K. Izzo, and Z. I. Johnson. 2013. Relationship between abundance and specific activity of bacterioplankton in open ocean surface waters. Appl. Environ. Microbiol. **79**: 177–184. doi:10.1128/AEM.02155-12

Jephcott, T. G., C. Alves-De-Souza, F. H. Gleason, F. F. Ogtrop, T. Sime-Ngando, S. A. Karpov, and L. Guillou. 2016. Ecological impacts of parasitic chytrids, syndiniales and perkinsids on populations of marine photosynthetic dinoflagellates. Fungal Ecol. **19**: 47–58. doi:10.1016/j.funeco.2015.03.007

Johnson, Z. I., E. R. Zinser, A. Coe, N. P. Mcnulty, E. M. S. Woodward, and S. W. Chisholm. 2006. Niche partitioning among *Prochlorococcus* ecotypes along ocean-scale environmental gradients. Science. **311**: 1737–1740. doi:10.1126/science.1118052

Kaneko, H., I. Yasuda, K. Komatsu, and S. Itoh. 2013. Observations of vertical turbulent nitrate flux across the Kuroshio. Geophys. Res. Lett. **40**: 3123–3127. doi:10.1002/grl.50613

Kashtan, N., and others. 2014. Single-Cell Genomics Reveals Hundreds of Coexisting Subpopulations in Wild

Prochlorococcus. Science. **344**: 416–420. doi:10.1126/science.1248 575

Kirkham, A. R., C. Lepère, L. E. Jardillier, F. Not, H. Bouman, A. Mead, and D. J. Scanlan. 2013. A global perspective on marine photosynthetic picoeukaryote community structure. ISME J. **7**: 922–936. doi:10.1038/ismej.2012.166

Larkin, M. A., and others 2007. Clustal W and Clustal X version 2.0. Bioinformatics. **23**: 2947–2948. doi:10.1093/bioinformatics/btm404

Lévy, M., R. Ferrari, P. J. S. Franks, A. P. Martin, and P. Rivière. 2012. Bringing physics to life at the submesoscale. Geophys. Res. Lett. **39**: L14602. doi:10.1029/2012GL052756

Lin, Y. C., T. Campbell, C. C. Chung, G. C. Gong, K. P. Chiang, and A. Z. Worden. 2012. Distribution patterns and phylogeny of marine stramenopiles in the north pacific ocean. Appl Environ Microbiol. **78**: 3387–3399. doi:10.1128/AEM.06952-11

Marin, B., and M. Melkonian. 2010. Molecular phylogeny and classification of the Mamiellophyceae class. nov. (Chlorophyta) based on sequence comparisons of the nuclear- and plastid-encoded rRNA operons. Protist. **161**: 304–336. doi:10.1016/j.protis.2009.10.002

Massana, R. 2011. Eukaryotic picoplankton in surface oceans. Annu. Rev. Microbiol. **65**: 91–110. doi:10.1146/annurev-micro-090110-102903

Massana, R., J. Del Campo, M. E. Sieracki, S. Audic, and R. Logares. 2014. Exploring the uncultured microeukaryote majority in the oceans: reevaluation of ribogroups within stramenopiles. ISME J. **8**: 854–66. doi:10.1038/ismej.2013.204

Menden-Deuer, S., and J. Rowlett. 2014. Many ways to stay in the game: individual variability maintains high biodiversity in planktonic microorganisms. J R Soc Interface. **11**: 20140031. doi:10.1098/rsif.2014.0031

Monier, A., A. Z. Worden, and T. A. Richards. 2016. Phylogenetic diversity and biogeography of the Mamiellophyceae lineage of eukaryotic phytoplankton across the oceans. Environ Microbiol Rep. **8**: 461–469. doi:10.1111/1758-2229.12390

Moon-Van Der Staay, S. Y., R. De Wachter, and D. Vaulot. 2001. Oceanic 18S rDNA sequences from picoplankton reveal unsuspected eukaryotic diversity. Nature. **409**: 607–10. doi:10.1038/35054541

Mugo, R. M., S. I. Saitoh, F. Takahashi, A. Nihira, and T. Kuroyama. 2014. Evaluating the role of fronts in habitat overlaps between cold and warm water species in the western North Pacific: A proof of concept. Deep Sea Res., Part II. **107**: 29–39. doi:10.1016/j.dsr2.2013.11.005

Nagai, T., A. Tandon, H. Yamazaki, and M. J. Doubell. 2009. Evidence of enhanced turbulent dissipation in the frontogenetic Kuroshio Front thermocline. Geophys. Res. Lett. **36**: L12609, doi:10.1029/2009GL038832

Nagai, T., A. Tandon, H. Yamazaki, M. J. Doubell, and S. Gallager. 2012. Direct observations of microscale turbulence and thermohaline structure in the Kuroshio Front. J. Geophys. Res. **117**: C08013, doi:10.1029/2011JC007228

Nishibe, Y., K. Takahashi, T. Shiozaki, S. Kakehi, H. Saito, and K. Furuya. 2014. Size-fractionated primary production in the Kuroshio Extension and adjacent regions in spring. J. Oceanogr. **71**: 27–40.

Omand, M. M., E. A. D'Asaro, C. M. Mary, J. Perry, N. Briggs, I. Cetinić, and A. Mahadevan. 2015. Eddy-driven subduction exports particulate organic carbon from the spring bloom. Science. **348**: 222–225. doi:10.1126/science.1260062

Palevsky, H. I., F. Ribalet, J. E. Swalwell, C. E. Cosca, E. D. Cokelet, R. A. Feely, E. Virginia Armbrust, and P. D. Quay. 2013. The influence of net community production and phytoplankton community structure on CO_2 uptake in the Gulf of Alaska. Global Biogeochem. Cycles. **27**: 664–676. doi:10.1002/gbc.20058

Pollard, R. T., and L. A. Regier. 1992. Vorticity and vertical circulation at an ocean front. J. Phys. Oceanogr. **22**: 609–625. doi:10.1175/1520-0485(1992)022Ã0609:VAVCAAÎ2.0.CO;2

Qiu, B. 2001. Kuroshio and Oyashio currents, 1413–25 In J. H. Steele, S. A. Thorpe and K. K. Turekian [eds.], Ocean currents: a derivative of the encyclopedia of ocean sciences. Academic Press.

Ribalet, F., and others. 2010. Unveiling a phytoplankton hotspot at a narrow boundary between coastal and offshore waters. Proc. Natl. Acad. Sci. U. S. A. **107**: 16571–16576. doi:10.1073/Pnas.1005638107

Rii, Y. M., S. Duhamel, R. R. Bidigare, D. M. Karl, D. J. Repeta, and M. J. Church. 2016. Diversity and productivity of photosynthetic picoeukaryotes in biogeochemically distinct regions of the South East Pacific Ocean. Limnol. Oceanogr., **61**: 806824. doi:10.1002/lno.10255

Rodriguez, F., E. Derelle, L. Guillou, F. Le Gall, D. Vaulot, and H. Moreau. 2005. Ecotype diversity in the marine picoeukaryote *Ostreococcus* (Chlorophyta, Prasinophyceae). Environ. Microbiol. **7**: 853–859. doi:10.1111/j.1462-2920.2005.00758.x

Schaum, E., B. Rost, A. J. Millar, and S. Collins. 2012. Variation in plastic responses of a globally distributed picoplankton species to ocean acidification. Nat. Clim. Change. **3**: 298–302. doi:10.1038/nclimate1774

Shi, X. L., C. Lepere, D. J. Scanlan, and D. Vaulot. 2011. Plastid 16S rRNA gene diversity among eukaryotic picophytoplankton sorted by flow cytometry from the South Pacific Ocean. PloS one. **6**: e18979. doi:10.1371/journal.pone.0018979

Simmons, M. P., C. Bachy, S. Sudek, M. J. van Baren, L. Sudek, M. Ares, and A. Z. Worden. 2015. Intron invasions trace algal speciation and reveal nearly identical Arctic

and Antarctic *Micromonas* populations. Mol. Biol. Evol. **32**: 2219–2235. doi:10.1093/molbev/msv122

Simmons, M. P., and others. 2016. Abundance and biogeography of picoprasinophyte ecotypes and other phytoplankton in the Eastern North Pacific Ocean. Appl Environ Microbiol. **82**: 1693–1705. doi:10.1128/AEM.02730-15

Slapeta, J., P. Lopez-Garcia, and D. Moreira. 2006. Global dispersal and ancient cryptic species in the smallest marine eukaryotes. Mol. Biol. Evol. **23**: 23–29.

Subirana, L., and others. 2013. Morphology, genome plasticity, and phylogeny in the genus *Ostreococcus* reveal a cryptic species, *O. mediterraneus* sp. nov. (Mamiellales, Mamiellophyceae). Protist. **164**: 643–659. doi:10.1016/j.protis.2013.06.002

Taylor, A. G., R. Goericke, M. R. Landry, K. E. Selph, D. A. Wick, and M. J. Roadman. 2012. Sharp gradients in phytoplankton community structure across a frontal zone in the California Current Ecosystem. J. Plankton Res. **34**: 778–789. doi:10.1093/plankt/fbs036

Van Baren, M. J., and others. 2016. Evidence-based green algal genomics reveals marine diversity and ancestral characteristics of land plants. BMC Genomics. **17**: 267. doi:10.1186/s12864-016-2585-6

Vaulot, D., W. Eikrem, M. Viprey, and H. Moreau. 2008. The diversity of small eukaryotic phytoplankton ($\leq$3 μm) in marine ecosystems. FEMS Microbiol. Rev. **32**: 795–820. doi:10.1111/j.1574-6976.2008.00121.x

Worden, A. Z. 2006. Picoeukaryote diversity in coastal waters of the Pacific Ocean. Aquat. Microbial Ecol. **43**: 165–175. doi:10.3354/ame043165

Worden, A. Z., J. K. Nolan, and B. Palenik. 2004. Assessing the dynamics and ecology of marine picophytoplankton: The importance of the eukaryotic component. Limnol Oceanogr. **49**: 168–179. doi:10.4319/lo.2004.49.1.0168

Worden, A. Z., and F. Not. 2008. Ecology and diversity of picoeukaryotes. In D. L. Kirchman [ed.], Microbial ecology of the oceans. John Wiley & Sons, Inc.

Worden, A. Z., and others. 2009. Green evolution and dynamic adaptations revealed by genomes of the marine picoeukaryotes Micromonas. Science. **324**: 268–272.

Worden, A. Z., M. J. Follows, S. J. Giovannoni, S. Wilken, A. E. Zimmerman, and P. J. Keeling. 2015. Environmental science. Rethinking the marine carbon cycle: Factoring in the multifarious lifestyles of microbes. Science. **347**: 1257594. doi:10.1126/science.1257594

Yamamoto, T. 1986. Small-scale variations in phytoplankton standing stock and productivity across the oceanic fronts in the Southern Ocean. Mem. Natl. Inst. Polar Res., Spec. **40**: 25–41. Issue (Jpn.)

Yamamoto, T., S. Nishizawa, and A. Taniguchi. 1988. Formation and retention of phytoplankton peak abundance in the Kuroshio Front. J. Plankton Res. **10**: 1113–1130. doi:10.1093/plankt/10.6.1113

Acknowledgments

The authors thank T Nagai and H Yamazaki for providing a berth for SC on the R/V Natsushima, as well as the captain and crew and students from the Tokyo University of Marine Science and Technology who assisted with sample collection. They thank S Sudek for support for qPCR. YCL was supported at MBARI and UCSC by a Visiting Scientist Fellowship (NSC98-2917-I-019-101) from the National Science Council, Taiwan. They are grateful for support from the David and Lucile Packard Foundation (AZW), NSF- IOS0843119 (AZW), NSF-OCE 1048926 (MJF), Gordon and Betty Moore Foundation grants GBMF3788 (AZW), GBMF3778 (MJF), the MIT Hayashi Seed Fund (MJF and SC) the MIT Student Research Fund (SC), the MIT Houghton Fund (SC), and the Simons Collaborative for Ocean Processes and Ecology (MJF).

Conflict of Interest

None declared.

Submitted 22 October 2015
Revised 20 April 2016
Accepted 20 June 2016

Associate editor: Susanne Menden-Deuer